J Appl Physiol 95: 2453–2461, 2003.
First published August 22, 2003; 10.1152/japplphysiol.00303.2003.

Independent cerebral vasoconstrictive effects of hyperoxia and accompanying arterial hypocapnia at 1 ATA

Thomas F. Floyd,[1] James M. Clark,[2] Robert Gelfand,[2] John A. Detre,[3] Sarah Ratcliffe,[4] Dimitri Guvakov,[1] Christian J. Lambertsen,[2] and Roderic G. Eckenhoff[1]

[1]*Department of Anesthesia, and* [2]*Institute for Environmental Medicine Environmental Biomedical Stress Data Center, and* [3]*Departments of Neurology and* [4]*Biostatistics, University of Pennsylvania School of Medicine, Philadelphia, Pennsylvania 19104*

Submitted 25 March 2003; accepted in final form 20 August 2003

Floyd, Thomas F., James M. Clark, Robert Gelfand, John A. Detre, Sarah Ratcliffe, Dimitri Guvakov, Christian J. Lambertsen, and Roderic G. Eckenhoff. Independent cerebral vasoconstrictive effects of hyperoxia and accompanying arterial hypocapnia at 1 ATA. *J Appl Physiol* 95: 2453–2461, 2003. First published August 22, 2003; 10.1152/japplphysiol.00303.2003.—Breathing 100% O_2 at 1 atmosphere absolute (ATA) is known to be associated with a decrease in cerebral blood flow (CBF). It is also accompanied by a fall in arterial P_{CO_2} leading to uncertainty as to whether the cerebral vasoconstriction is totally or only in part caused by arterial hypocapnia. We tested the hypothesis that the increase in arterial P_{O_2} while O_2 was breathed at 1.0 ATA decreases CBF independently of a concurrent fall in arterial P_{CO_2}. CBF was measured in seven healthy men aged 21–62 yr by using noninvasive continuous arterial spin-labeled-perfusion MRI. The tracer in this technique, magnetically labeled protons in blood, has a half-life of seconds, allowing repetitive measurements over short time frames without contamination. CBF and arterial blood gases were measured while breathing air, 100% O_2, and 4 and 6% CO_2 in air and O_2 backgrounds. Arterial P_{O_2} increased from 91.7 ± 6.8 Torr in air to 576.7 ± 18.9 Torr in O_2. Arterial P_{CO_2} fell from 43.3 ± 1.8 Torr in air to 40.2 ± 3.3 Torr in O_2. CBF-arterial P_{CO_2} response curves for the air and hyperoxic runs were nearly parallel and separated by a distance representing a 28.7–32.6% decrement in CBF. Regression analysis confirmed the independent cerebral vasoconstrictive effect of increased arterial P_{O_2}. The present results also demonstrate that the magnitude of this effect at 1.0 ATA is greater than previously measured.

cerebral blood flow; oxygen; carbon dioxide; arterial spin-labeling; magnetic resonance; atmospheres absolute

CEREBRAL BLOOD FLOW (CBF) in normal subjects is under the continuous dominant control of arterial P_{CO_2} (Pa_{CO_2}), but it can be modulated by the background level of arterial P_{O_2} (Pa_{O_2}). Acute exposure to a high inspired P_{O_2} results in a cascade of physiological events leading to increased brain tissue P_{CO_2}, increased ventilation, decreased Pa_{CO_2}, and decreased CBF (29, 30). The magnitude of the decrease in CBF in response to breathing 100% O_2 at 1.0 atmosphere absolute (ATA), as measured by different methods, ranges from 13 to 27% of the air-breathing value. With the use of the Kety-Schmidt method, a 13–15% decrement has been measured (27, 34), whereas with ^{133}Xenon scintigraphy, a 21% decrease has been reported (40). Two recently reported MRI studies using phase contrast angiography found this decrease in CBF to be in the range of 16–27% (49, 59). Because breathing O_2, even at 1.0 ATA, is associated with arterial hypocapnia, it remains unclear whether the decreased CBF during hyperoxia is a consequence of the hypocapnia alone or whether there are separate effects of hypocapnia and hyperoxia. We tested the hypothesis that an increase in Pa_{O_2} while breathing O_2 at 1.0 ATA decreases CBF independently of the accompanying fall in Pa_{CO_2} using a noninvasive MRI method to measure CBF. Although the CO_2 and O_2 effects on CBF are physiologically inseparable, measurements of CBF over a range of Pa_{CO_2} values in air and O_2 backgrounds made it possible to determine their separate influences analytically.

METHODS

The experimental protocol was approved by the institutional review board, and informed consent was obtained from each subject. Seven men between the ages of 21 and 62 yr (mean ± SE: 39 ± 14 yr) were studied after medical history and physical examination determined no occult cardiovascular, respiratory, neurological, or psychiatric disorder.

An open breathing system was employed to deliver mixed gases by using a low dead space, nonrebreathing valve (Hans Rudolph model 1400) and 100-liter Douglas bag as the inspiratory reservoir. Premixed gases in high-pressure cylinders containing air, 4 and 6% CO_2 in air, and 4 and 6% CO_2 in O_2 were obtained from BOC Gases (Murray Hill, NJ). O_2 (100% O_2) was administered from the hospital wall supply. These gases were selected to provide comparable ranges of Pa_{CO_2} in air and O_2 backgrounds.

The experimental protocol was designed to minimize subject time in the magnet yet allow for stabilization of CBF after the inspired gas mixture was changed. The study was divided into two runs, an "air" run and a "hyperoxic" run. At the initiation of each run, a 10-min period of breathing was

Address for reprint requests and other correspondence: T. F. Floyd, Dept. of Anesthesia, Section of Cardiovascular & Thoracic Anesthesia, Hospital of the Univ. of Pennsylvania, 4-Dulles, 3400 Spruce St., Philadelphia, PA 19104-4283 (E-mail: floydt@uphs.upenn.edu).

The costs of publication of this article were defrayed in part by the payment of page charges. The article must therefore be hereby marked "*advertisement*" in accordance with 18 U.S.C. Section 1734 solely to indicate this fact.

allowed for CBF stabilization while subjects breathed either 21% O_2 (air run) or 100% O_2 (hyperoxic run). Subsequently, when gases were inspired containing increasing concentrations of CO_2, a 5-min period for stabilization on the new gas was allowed. A continuous arterial spin-labeled (CASL)-perfusion-MRI imaging session of 6 min followed stabilization on each gas for the purpose of measuring CBF. CBF measurements occurred in the following order: air run: *1*) air → *2*) air-4% CO_2 → *3*) air-6% CO_2; hyperoxic run: *4*) 100% O_2 → *5*) 96% O_2-4% CO_2→ *6*) 94% O_2-6% CO_2.

For arterial blood sampling, a 22- or 20-gauge radial arterial catheter was placed by using sterile technique and 2 ml of 1% lidocaine for local anesthesia. Arterial blood gas samples were withdrawn near the end of the 6-min MRI scanning phase. The 3-ml sample was placed in ice water and analyzed within 2–3 min of sampling by using a NOVA pHOX analyzer (NOVA Biomedical, Waltham, MA). The following parameters were measured: P_{O_2}, P_{CO_2}, pH, hemoglobin, and Hct. Arterial blood O_2 content (Ca_{O_2}) was calculated.

The duration of each run was ~40 min, including time for structural imaging. Subjects were allowed a 15- to 30-min rest period in air between the two runs.

CBF measurements were made by using the CASL-perfusion MRI method (4, 12, 16). This technique has been demonstrated in humans to have a high degree of accuracy compared with PET methods (65) as well as a high degree of precision (19). All CASL-perfusion MRI studies were performed in a 1.5-T GE Signa Echospeed scanner (GE Medical Systems, Milwaukee, WI). CASL control labeling was applied at the level of the cervicomedullary junction by using a postlabeling delay of 1.5 s (2). Images were acquired by using a gradient-echoplanar sequence [field of view = 24 × 15 cm, matrix 64 × 40, bandwidth 62.5 kHz, repitition time/echo time = 4,000/22 ms, slice thickness = 8 mm with a 2-mm gap]. Eight slices were acquired from inferior to superior in an interleaved order, and each slice acquisition took 45 ms. The imaging volume was chosen to include supratentorial structures. Each perfusion measurement consisted of 90 acquisitions with a scan time of ~6 min. Raw image data were saved onto DAT tape. A 1-min chemical shift image sequence was also performed to obtain data used for correcting geometric distortion in echoplanar images.

CASL-perfusion MRI data were reconstructed from raw data offline and corrected for geometric distortion by using custom software written in the Interactive Data Language software program (Research Systems, Boulder, CO). The reconstructed images in each scan were separated into 45 pairs of label and control images and then pairwise subtracted (1). The resulting series of 45 perfusion difference images were corrected for motion and physiological fluctuation by using an algorithm based on principal component analysis (3), followed by averaging across the image series to produce a single set of perfusion-sensitive images.

Absolute CBF was quantified from the mean difference perfusion images by using a modification of a previous approach (2) according to the following equation (12)

$$CBF = \frac{S_{CASL}\left[1 - \exp\left(\frac{-TR}{T1_{CSF}}\right)\right]}{S_{CSF}\lambda\rho} \frac{\exp\left(\frac{w}{T1_a}\right)\exp\left(\frac{TE}{T2_a}\right)}{2\alpha T1_a}$$

where S_{CASL} is the difference between the control and labeled image intensities, S_{CSF} is the average intensity of the control image in the manually defined ventricular region, $T1_{CSF}$ (4.2 s) is the longitudinal relaxation time of CSF, T1a and T2a are the longitudinal and transverse relaxation times of arterial blood, respectively, w is the postlabeling delay (1.5 s), α is the labeling efficiency (71%), λ is the water fraction of arterial blood (0.76), and ρ is the density of brain tissue (1.05 g/ml). $T1_a$ and $T2_a$ are assumed to be constant for this study at $T1_a$ = 1,100 ms and $T2_a$ = 240 ms. Use of fixed T1a rather than measuring tissue T1 assumes that the labeled spins remain primarily in the microvasculature rather than exchanging completely with tissue water. However, because blood and brain T1 values are almost equal at 1.5 T, violations of this assumption would cause only a small error. The CASL-perfusion MRI technique, therefore, measures the rate of microvascular blood flow within brain parenchyma (12). An example of quantitative perfusion images obtained from a 6-min acquisition is shown in Fig. 1.

Global CBF (CBF_{Global}) was determined by averaging perfusion values across all brain voxels. Second, brains were segmented into gray and white matter pixels based on the algorithm of Ashburner and Friston (7) within statistical parametric mapping (SPM) 99 (54a). CBF was determined for each tissue type yielding gray matter CBF (CBF_{Gray}) and white matter CBF (CBF_{White}).

Statistical analysis was performed by using JMP professional software version 5 (SAS, Cary, NC). The paired *t*-test was used to estimate differences in means for paired gas samples between runs. Multiple linear regression methods were used to model the contributions of baseline CBF during air breathing ($CBF_{Air\text{-}4\text{–}6\%}$), change in Pa_{CO_2} (ΔPa_{CO_2}), and change in Pa_{O_2} (ΔPa_{O_2}), to the change in CBF (ΔCBF) when moving between the paired gases (air-4% CO_2 → 96% O_2-4% CO_2, and air-6% CO_2 → 94% O_2-6% CO_2). Terms, P values, and power estimates are presented for this analysis.

Multiple linear and nonlinear regression approaches were also used to model the effects of baseline CBF while breathing 21% O_2 (CBF_{Air}), ΔPa_{CO_2} from baseline on 21% O_2, and $\Delta Pa_{O_2}$from baseline on 21% O_2, on CBF_{Gray}, CBF_{White}, and whole brain. Coefficients of determination (R^2) are presented for the models along with P values for each partial regression coefficient from ANOVA. A probability of $P \leq 0.05$ was chosen to test significance for the whole model and for partial regression coefficients.

RESULTS

All subjects completed the study. Figure 1 depicts a series of colorized CASL-perfusion MRI image sets used for CBF measurements in a single subject. Qualitatively, from visual inspection of the images, it can be seen that CBF increases during the air run with the addition of increasing inspired P_{CO_2}. Also, when the air and hyperoxic runs are compared, the matched pairs of images reveals the lower levels of CBF at all pairings in the hyperoxic run.

Table 1 summarizes the P_{CO_2}, P_{O_2}, Ca_{O_2}, as well as CBF_{Global}, CBF_{Gray}, and CBF_{White} regions. Breathing 100% O_2 vs. air at 1 Atm was associated with a relative hypocapnia or decrement in Pa_{CO_2} of ~3 Torr (P = 0.01). The mean relative differences in CBF_{Global} in the group pairings (n = 7) of air vs. 100% O_2, air-4% CO_2 vs. 96% O_2-4% CO_2, and air-6% CO_2 vs. 94% O_2-6%C O_2 were −32.6% ($P < 0.0001$), −28.7% ($P = 0.0008$), and −29.4% ($P < 0.0001$), respectively. It is important to note that, although there exists a statistical difference in Pa_{CO_2} tensions between the air and 100% O_2 exposures, by the addition of CO_2 at 4 and 6% inspired concentrations, we were able to eliminate any statisti-

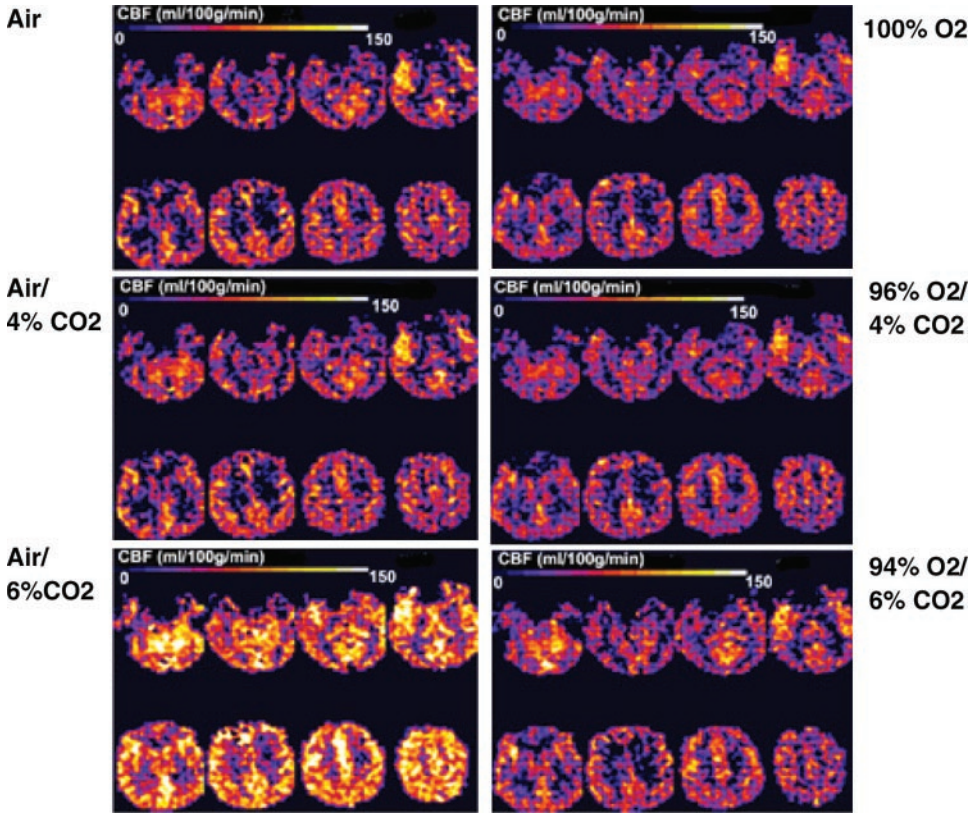

Fig. 1. Colorized continuous arterial spin labeled (CASL)-perfusion MRI images with scale depicting cerebral blood flow (CBF) changes in response to air, air-4% CO_2, air-6% CO_2, 100% O_2, 96% O_2-4% CO_2, and 94% O_2-6% CO_2.

cal differences in these levels in the subsequent comparisons.

The major goal of this study was to determine whether the effects of Pa_{O_2} and Pa_{CO_2} on CBF could be discriminated and identify whether O_2 has a vasoconstrictive effect on CBF independent of the mild arterial hypocapnia, which occurs in response to hyperoxia in normal subjects at rest. Figure 2 depicts graphically the relationship between CBF and Pa_{CO_2} for the seven subjects while breathing air or O_2 background gases alone and then with 4 and 6% CO_2. Two distinct, nearly parallel curves are defined. The initial points on each curve depict a difference in CBF while breathing air vs. 100% O_2. As mentioned above, Pa_{CO_2} is decreased during the transition from air breathing to O_2 breathing at 1.0 ATA resulting in the shift of the lower (hyperoxic run) curve to the left. Any difference in CBF between these initial study points (air vs. 100% O_2) thus reflects the combined effects of arterial hypocapnia and hyperoxia on the cerebral vasculature (Table 1). With the addition of 4 and 6% CO_2, mean differences in Pa_{CO_2} when breathing the air or hyperoxic mixtures were not significant (Table 1), and the differences between the curves at these points of comparison essentially reflect the effect of the difference in Pa_{O_2} alone.

Preliminary univariate analysis indicated that the absolute magnitude and the percentage of the decrease in CBF in response to hyperoxic breathing are also dependent on the baseline level of CBF during air breathing (Fig. 3). Therefore, multiple regression anal-

Table 1. *Arterial P_{CO_2}, O_2 content, and CBF by inspired gas*

Inspired Gas	P_{CO_2}, Torr	P_{O_2}, Torr	Ca_{O_2}, ml/dl	CBF_{Global}, ml·100 g^{-1}·min^{-1}	CBF_{Gray}, ml·100 g^{-1}·min^{-1}	CBF_{White}, ml·100 g^{-1}·min^{-1}
Air-21% O_2*	43.3 ± 1.8 (P = 0.01)	91.7 ± 6.8 (P < 0.0001)	17.9 ± 0.8 (P < 0.0001)	53.6 ± 6.8 (P < 0.0001)	68.6 ± 8.9 (P < 0.0001)	39.6 ± 7.7 (P = 0.003)
Air-4% CO_2†	46.4 ± 1.7 (P = 0.25)	127.0 ± 5.4 (P < 0.0001)	18.5 ± 0.9 (P = 0.0002)	56.1 ± 10.5 (P = 0.0008)	73.5 ± 13.7 (P = 0.003)	39.8 ± 11.8 (P = 0.03)
Air-6% CO_2‡	52.1 ± 1.6 (P = 0.13)	144.5 ± 6.6 (P < 0.0001)	18.7 ± 0.8 (P < 0.0001)	70.1 ± 6.4 (P < 0.0001)	90.4 ± 11.9 (P < 0.0001)	47.6 ± 4.5 (P = 0.006)
100% O_2	40.2 ± 3.3	576.7 ± 18.9	20.3 ± 1.1	36.1 ± 4.9	46.6 ± 5.3	27.8 ± 3.8
96% O_2-4% CO_2	45.6 ± 2.2	580.2 ± 19.6	20.2 ± 0.8	40.0 ± 3.1	50.3 ± 5.8	30.5 ± 5.1
94% O_2-6% CO_2	51.1 ± 2.0	579.4 ± 10.6	20.3 ± 0.8	49.6 ± 5.4	62.4 ± 8.3	35.2 ± 8.6

Values are means ± SD. CBF, cerebral blood flow; Ca_{O_2}, arterial O_2 content; CBF_{Global}, global CBF; CBF_{Gray}, CBF in gray matter; CBF_{White}, CBF in white matter. *Significance in comparison between air (21% O_2) and 100% O_2. †Significance in comparison between air-4% CO_2 and 96% O_2-4% CO_2. ‡Significance in comparison between air-6% CO_2 and 94% O_2-6% CO_2.

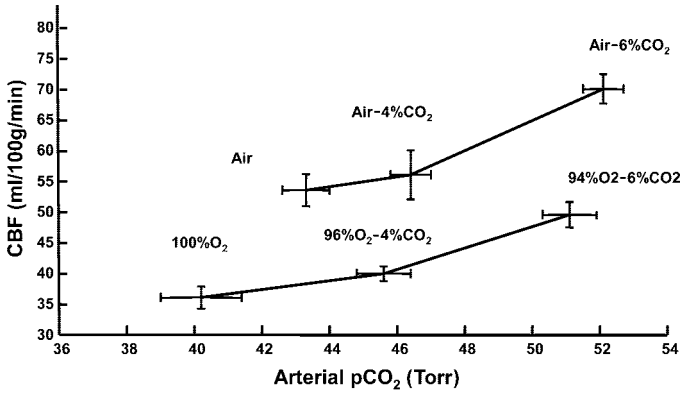

Fig. 2. CBF is plotted vs. arterial P_{CO_2} for the air and hyperoxia runs. Values are means ± SE for CBF and P_{CO_2} values for each gas. Means are connected to describe curves representing the CBF response to P_{CO_2} in the presence of air and hyperoxia.

ysis of the change in CBF when moving from air-4% CO_2 → 96% O_2-4% CO_2 and air-6% CO_2 → 94% O_2-6% CO_2 ($\Delta CBF_{4-6\%}$) was conducted as a function of the initial CBF during the breathing of air-4% CO_2 or air-6% CO_2 ($CBF_{Air-4-6\%}$), ΔPa_{O_2}, and ΔPa_{CO_2} during the same transitions. A statistical summary for each of the covariates is listed in Table 2. It can be seen then that both $CBF_{Air-4-6\%}$ ($P = < 0.0001$) and ΔPa_{O_2} ($P = 0.0081$) contribute significantly to the magnitude of ΔCBF. It can also be seen that any change in Pa_{CO_2} did not significantly contribute to ΔCBF because $P = 0.17$ for the covariate ΔPa_{CO_2}.

Thus, by comparing results at matched testing points, the decrease in CBF persists when the hypocapnia associated with breathing 100% O_2 has been eliminated (Table 1, Fig. 2). An independent cerebral vasoconstrictive effect of hyperoxia is also confirmed by using multiple regression analysis over the experimentally imposed ranges of Pa_{CO_2} and Pa_{O_2} and by accounting for the impact of baseline CBF when air was breathed on the magnitude of any change.

To examine the effects of hyperoxic breathing on different tissue types within the brain, multiple linear and nonlinear regression methods were used to analyze the contributions of the following covariates to CBF: $CBF_{Air-21\%}$ (baseline CBF on air, before the addition of CO_2), ΔPa_{O_2}, and ΔPa_{CO_2}.

Table 2. *ΔCBF multiple regression analysis*

Term	Coefficient	*P* Value	Power (α = 0.05)	Least Significant Number (α = 0.05)
Intercept	−14	0.0029	0.85	8
$CBF_{Air-4\%-6\%}$	0.70	<0.0001	>0.99	6
ΔP_{O_2}	−0.25	0.008	0.71	9
ΔP_{CO_2}	1.0	0.17	0.12	28

$n = 14$, which includes measurements of the change in CBF (ΔCBF) from 7 subjects who breathed air-4% CO_2 vs. 96%-4% CO_2 and air-6% CO_2 vs. 94% O_2-6% CO_2.

Regression models were created for global, gray matter, and white matter. The following equations resulted

$$CBF_{Global} = 0.62CBF_{Global\text{-}Air} - 0.034\Delta Pa_{O_2} + 1.5\Delta Pa_{CO_2} + 22 \quad (1)$$

which had model R^2 and *P* values of 0.84 and <0.0001, respectively, and individual *P* values of <0.0001 for CBF_{Air}, ΔPa_{O_2}, and ΔPa_{CO_2}, and a *P* value of 0.0043 for the intercept

$$CBF_{Gray} = 0.61CBF_{Gray\text{-}Air} - 0.048\Delta Pa_{O_2} + 1.2\Delta Pa_{CO_2} + 0.11\Delta Pa_{CO_2}{}^2 + 29 \quad (2)$$

which had model R^2 and *P* values of 0.89 and <0.0001, respectively, and individual *P* values of <0.0001 for CBF_{Air}, ΔPa_{O_2}, and ΔPa_{CO_2}, and *P* values of 0.0012 and 0.0088 for the intercept and $\Delta Pa_{CO_2}{}^2$, respectively, and

$$CBF_{White} = 0.73CBF_{White\text{-}Air} - 0.025\Delta Pa_{O_2} + 0.67\Delta Pa_{CO_2} + 11 \quad (3)$$

which had model R^2 and *P* values of 0.73 and <0.0001, respectively, and individual *P* values of <0.0001 for CBF_{Air} and ΔPa_{O_2}, and *P* values of 0.0029 and 0.0013 for the intercept and ΔPa_{CO_2}, respectively.

Plots of actual vs. predicted CBF values from the three models are further depicted in Fig. 4, *A–C*. The effect of a change in Pa_{O_2} could not be modeled in a nonlinear fashion because the P_{O_2} created in our experimental design essentially represents only two levels (high and low) in the presence of air breathing or 100% O_2 breathing. Nonlinear modeling of CO_2 ten-

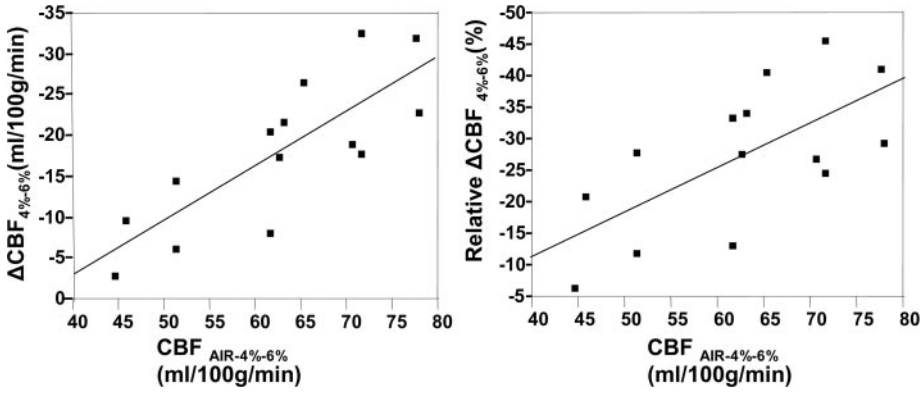

Fig. 3. Absolute (*left*) and relative (*right*) changes in CBF from baseline measurements made on 4 and 6% CO_2 ($\Delta CBF_{4-6\%}$) in air background to measurements made on 4 and 6% CO_2 in O_2 background are plotted vs. baseline CBF measurements made on 4–6% CO_2 in air background.

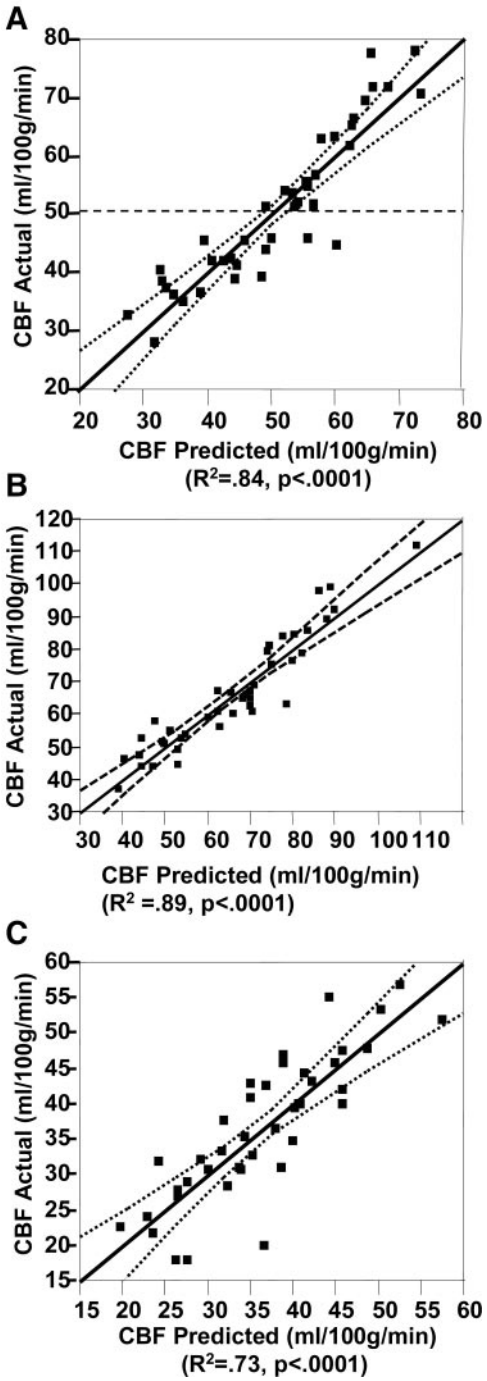

Fig. 4. Actual (measured) CBF vs. predicted (model derived) CBF for global (*A*), gray matter (*B*), and white matter (*C*) along with 95% confidence intervals (dotted lines).

sions was attempted for global, gray, and white matter and demonstrated significance when modeled as a binomial in gray matter alone.

DISCUSSION

Independent cerebral vasoconstrictive effect of hyperoxia. As stated previously, the normal CO_2-related interaction of respiratory and cerebral circulatory control causes the concurrent effects of hyperoxia and arterial hypocapnia to be physiologically inseparable. The linkage of these effects has been attributed to hyperventilation induced by CO_2 retention in respiratory control centers (22, 31, 33) that is in turn caused by a reduced CO_2-carrying capacity of oxyhemoglobin in association with high concentrations of physically dissolved O_2 (Haldane effect) (38). Nevertheless, the present results (Fig. 2) clearly demonstrate an independent cerebral vasoconstrictive effect of hyperoxia across a wide range of Pa_{CO_2}. In agreement, Kolbitsch et al. (28) recently demonstrated a significant reduction in regional CBF during oxygen breathing at 1.0 ATA when end-tidal (alveolar) P_{CO_2} was maintained at the air-breathing control level. Reivich (45, 46) also found what appeared to be an independent vasoconstrictor effect of hyperoxia during oxygen breathing at 3.5 ATA with Pa_{CO_2} maintained at ~15 Torr by voluntary hyperventilation. Similar results were observed at 2.0 ATA with P_{CO_2} maintained at ~19 Torr.

In contrast to the above results, an independent vasoconstrictor effect of hyperoxia is not supported by the observations that CBF remained unchanged in normal men during the transition from air breathing to 80% O_2 at 1.0 ATA with alveolar P_{CO_2} controlled at 43 Torr (29, 30) or in unanesthetized ponies breathing O_2 at 1.0 ATA with Pa_{CO_2} maintained at air-breathing control levels (10). The known association of cerebral hypoxia with extreme hypocapnia during air breathing (46) suggests that the apparent independent vasoconstrictor effect of hyperoxia found by Reivich at hypocapnic levels of Pa_{CO_2} could also be explained by removal of the cerebral vasodilator effect of hypoxia (30, 45).

Analysis of the present data also demonstrates an independent vasoconstrictor effect of hyperoxia on CBF_{Gray} and CBF_{White} as well as on CBF_{Global}. The three linear models that were developed for the purpose of comparing the effects of hyperoxic breathing in global, gray, and white matter describe a greater vasoconstrictive response to increasing P_{O_2} and greater vasodilatory response to increasing P_{CO_2} in gray vs. white matter. Gray matter is metabolically more active than white matter, and thus these differences are not surprising. The higher CBF values recorded for gray matter and lower values for white matter (Table 1) are consistent with values recorded for PET (65) during air breathing. The CBF_{Gray}-to-CBF_{White} ratio of 1.7 from our present work is consistent with findings in the literature from previous work using PET and single-photon-emission computed tomography of 1.6–1.8 (24, 25, 41).

O_2 in the regulation of CBF. Mechanisms proposed as involved in the localized regulation of CBF in response to hyperoxia and hypoxia are complex and may include roles for the parenchyma (43, 51), cerebrovascular endothelium (15, 18, 42), specific brain O_2-sensitive neurons (23), and even the red blood cells (17). When Pa_{O_2} is reduced by reducing the inspired P_{O_2}, CBF does not increase until Pa_{O_2} is <50 Torr (30, 46). In contrast, CBF has been shown to inversely correlate with Ca_{O_2} when Ca_{O_2} is low due to reduced hemoglobin

concentration and Pa_{O_2} is not manipulated (9). This correlation occurs whether O_2 is carried by the intact red blood cells or in a dissolved state(58). In the present report, there was also an inverse relation between Ca_{O_2} and CBF. When inspired percent O_2 was increased from 21 to 100% at 1.0 ATA, there was a 13–14% increase in Ca_{O_2}, which was concurrent with a 33% decrease in CBF. Although these correlations exist, they do not necessarily mean that Ca_{O_2} acts as a specific factor in brain O_2 flow control. Rather, it has been suggested that Po_2-dependent cells in endothelium may act as local O_2 sensors modulating vascular tone (44). The vasoconstrictive effect of hyperoxia may be related to inactivation of NO by enhanced generation of O_2-free radicals(44).

Magnitude of hyperoxic cerebral vasoconstriction. In the present study, the transition from breathing air to 100% O_2 at 1.0 ATA caused a larger decrease in CBF (33%) than the 13–15% decrement, which has been consistently reported previously (27, 34) by using the Kety-Schmidt technique, or the 21% decrease reported by Ohta (40) by using ^{133}Xe scintigraphy. The present results are more consistent with, yet still larger than, the 16–27% decrease in CBF during O_2 breathing at 1.0 ATA recently reported by Watson (59) and Rostrup (49) by using another MRI technique, dynamic susceptibility contrast. Even during O_2 breathing at 3.5 ATA, a previously reported CBF decrement of 25% (34) is smaller than the present value for O_2 breathing at 1.0 ATA. Only a few studies contain CBF measurements during O_2 breathing at >1 ambient pressure. Lambertsen et al. (34) found CBF decrements of 15 and 25% at 1.0 and 3.5 ATA, respectively, whereas Reivich (45, 46) reported values of 22 and 27% at 2.0 and 3.5 ATA, respectively, in the presence of arterial hypocapnia. More recently, Ohta (40) measured CBF decrements of 9, 21, 23, and 19% at O_2 pressures of 0.5, 1.0, 1.5, and 2.5 ATA, respectively. The latter results suggest that the cerebral vasoconstrictive effect of hyperoxia may be near maximal at 1.0 ATA. At the present time, it is not practical to use CASL-perfusion MRI or other MRI methods at ambient pressures that are >1 atm.

Comparison with previous CBF measurements. Quantitative investigation of CBF and metabolism in man became possible when Kety and Schmidt developed an inert gas method for measuring CBF by calculating rate of N_2O uptake by the brain (26). The method required repeated sampling of brain venous blood from the superior bulb of the internal jugular vein concurrently with arterial blood while the subject breathed 15% N_2O for at least 10 min. Subsequent demonstrations that cerebral O_2 consumption is not changed by O_2 breathing at 1.0 (27, 32) or 3.5 ATA (32) made it possible to use arterial-venous O_2 content differences across the brain to measure relative changes in CBF under these conditions (53). Continued investigation led to the development of additional CBF measurement methods that used other inert gas tracers or radioactive labels to determine rate of uptake of the tracer or rate of washout after a state of near saturation has been established (46). All of these methods require either the sampling of brain venous blood or the monitoring of brain venous concentrations of the selected tracer.

Blood from the internal jugular bulb is known to contain contributions from extracranial or extracerebral sources (52, 53). While air was breathed at 1.0 ATA, extracranial contributions to internal jugular venous flow have been estimated to range from 3 to 7% (52), with the occasional possibility of gross contamination from extracranial venous effluent (35). Scheinberg (50) found that contamination of cerebral venous blood by facial or neck blood caused falsely low values of CBF, arterio-venous O_2 difference, and O_2 consumption. He estimated that some degree of extracerebral contamination occurred in ~20% of the subjects. In contrast, the CASL-perfusion MRI technique allows CBF to be determined from designated intracranial sources by measuring the rate of microvascular blood flow within brain parenchyma (12).

It is possible, yet unlikely, that the potential extracerebral contamination of brain venous blood in some of the previous studies can account for the reported absence of an independent cerebral vasoconstrictive effect of hyperoxia or the smaller magnitude of this effect found previously. At the present time, there are no obvious explanations for the differences between the results of this study and those of previous investigations. In some aspects, the results of the present study are remarkably consistent with previous data. Average values of 53.6 ml · 100 g^{-1} · min^{-1} for CBF_{Global} at an Pa_{CO_2} of 43.3 Torr during air breathing (Table 1) are essentially identical to corresponding values of 53 ml · 100 g^{-1} · min^{-1} at 43 Torr in one of the subject groups studied by Kety and Schmidt (27). In addition, the average CBF value of 36.1 ml · 100 g^{-1} · min^{-1} at an Pa_{CO_2} of 40.2 Torr during O_2 breathing (Table 1) falls directly on the curve established for CBF vs. Pa_{CO_2} in an O_2 background while using cerebral clearance of ^{133}Xe to measure CBF (14).

Although the present CBF-Pa_{CO_2} relationships for both air and O_2 breathing without added CO_2 are consistent with the results of previous studies using other methods, the slopes of the present CBF-Pa_{CO_2} curves (Fig. 2) are more shallow than those found previously in normal subjects. Using arterio-venous O_2 differences across the brain to calculate relative changes in CBF during air breathing at 1.0 ATA, Lambertsen et al. (33) found that CBF increased by 57.6% for an Pa_{CO_2} increment of 8.9 Torr. During air breathing in the present study, CBF_{Global} increased by 30.8% for an 8.8-Torr increase in Pa_{CO_2} (Table 1). By using clearance of ^{133}Xe to measure CBF during O_2 breathing with added CO_2, CBF more than doubled (102.5%) for an Pa_{CO_2} increase of 11.4 Torr (14). Corresponding values for the present study during O_2 breathing were 37.4% and 10.9 Torr, respectively (Table 1).

Effect of CO_2 breathing on Pa_{O_2}. The breathing of CO_2 in an air background resulted in small increases in Pa_{O_2} from 91.7 ± 6.8 Torr on air to 127.0 ± 5.4 Torr on air-4% CO_2 and 144.5 ± 6.6 Torr on air-6% CO_2, as well as corresponding increments in Ca_{O_2} from 17.9 ±

0.8 ml/dl on air to 18.5 ± 0.9 ml/dl on air-4% CO_2 and 18.7 ± 0.8 ml/dl on air-6% CO_2, differences that were not observed during the breathing of CO_2 in an O_2 background (Table 1). An increase in Pa_{O_2} during air breathing with added CO_2 has been attributed to increased alveolar ventilation with improved alveolar ventilation-blood flow matching (55). The present average Pa_{O_2} values of 127.0 and 144.5 Torr at inspired P_{CO_2} levels of ~28 and 43 Torr agree well with previously measured values of 128.5 and 133.3 Torr at controlled inspired P_{CO_2} levels of 30 and 40 Torr, respectively (13).

CASL-perfusion MRI. CASL-perfusion MRI is ideally suited for this type of study at 1.0 ATA because it is completely noninvasive and the tracer, magnetically flipped protons in arterial blood, has a half-life on the order of several seconds. Multiple measurements can be obtained, over temporally short time frames, without contamination from retained tracer. Several excellent reviews have been published with detailed theoretical descriptions of the technique (8, 11, 61, 63).

The CASL-perfusion MRI technique has been validated against "gold standards" such as PET (37, 65) and dynamic susceptibility contrast MRI methods (36) in human brain studies. Calamante et al. (11) offer a detailed listing of CBF measurements in various species and comparisons with those made in the same species with more traditional methods, including microspheres. Walsh et al. (56) compared regional CBF measurements by using the arterial spin-labeling technique with those obtained from radioactive microspheres in the rat and found a mean difference of 1.5%. The CASL-perfusion MRI technique has been applied clinically to study CBF in stroke (12), epilepsy (60), and Alzheimer's dementia (6), as well as blood flow in other organ systems such as lung (39, 48), kidney (47), and muscle perfusion (21). The technique has been additionally utilized in human functional brain-mapping research (62), research into human cerebral physiology (20), and in the laboratory animal for the study of blood flow in various organ systems (54, 64).

The most significant concern for CASL-perfusion MRI is that prolonged arterial blood transit times, such as might exist in the presence of cerebrovascular disease, may cause an underestimation of flow (11). At the extreme, transit time could be greater than the time for the label to decay (T1). This deficiency has been exploited to assist in the diagnosis of cerebrovascular disease through the noninvasive mapping of inhomogeneities in regional CBF (57).

In conclusion, the observed decrease in CBF while breathing 100% O_2 at 1.0 ATA represents the combined effects of arterial hyperoxia and hypocapnia. Furthermore, the present data support the hypothesis that breathing O_2 at 1.0 ATA causes cerebral vasoconstriction independently of any vasoconstriction associated with the accompanying arterial hypocapnia. These data also document that gray matter cerebral vasculature is relatively more sensitive to the vasoconstrictive properties of hyperoxia and vasodilatory properties of hypercarbia over the ranges tested. The magnitude of hyperoxia-induced cerebral vasoconstriction is considerably greater than previously reported and is highly dependent on the magnitude of the baseline CBF. If the systemic vasculature responds to hyperoxia in a similar degree, these results have relevance to the use of hyperoxic inspired gas mixtures as an effective means for reducing decompression stress in undersea and aerospace medicine.

We acknowledge the assistance of Julio Gonzalez, David Alsop, and Joseph Maldjian for technical assistance on this project.

DISCLOSURES

This grant was supported by Navy contract no. N61331-99-C-0040.

REFERENCES

1. **Alsop D.** Correction of ghost artifacts and distortion in echo-planar MR imaging with an iterative reconstruction technique (Abstract). *Radiology* 197: 338, 1995.
2. **Alsop DC and Detre JA.** Reduced transit-time sensitivity in noninvasive magnetic resonance imaging of human cerebral blood flow. *J Cereb Blood Flow Metab* 16: 1236–1249, 1996.
3. **Alsop DC and Detre JA.** Reduction of excess noise in fMRI time series data using noise image templates (Abstract). *Proc Intl Soc Magn Reson Med* 5: 1687, 1997.
4. **Alsop DC and Detre JA.** Multisection cerebral blood flow MR imaging with continuous arterial spin labeling. *Radiology* 208: 410–416, 1998.
6. **Alsop DC, Detre JA, and Grossman M.** Assessment of cerebral blood flow in Alzheimer's disease by spin-labeled magnetic resonance imaging. *Ann Neurol* 47: 93–100, 2000.
7. **Ashburner J and Friston K.** Multimodal image coregistration and partitioning—a unified framework. *Neuroimage* 6: 209–217, 1997.
8. **Barbier EL, Lamalle L, and Decorps M.** Methodology of brain perfusion imaging. *J Magn Reson Imaging* 13: 496–520, 2001.
9. **Brown MM, Wade JP, and Marshall J.** Fundamental importance of arterial oxygen content in the regulation of cerebral blood flow in man. *Brain* 108: 81–93, 1985.
10. **Busija DW, Orr JA, Rankin JH, Liang HK, and Wagerle LC.** Cerebral blood flow during normocapnic hyperoxia in the unanesthetized pony. *J Appl Physiol* 48: 10–15, 1980.
11. **Calamante F, Thomas DL, Pell GS, Wiersma J, and Turner R.** Measuring cerebral blood flow using magnetic resonance imaging techniques. *J Cereb Blood Flow Metab* 19: 701–735, 1999.
12. **Chalela JA, Alsop DC, Gonzalez-Atavales JB, Maldjian JA, Kasner SE, and Detre JA.** Magnetic resonance perfusion imaging in acute ischemic stroke using continuous arterial spin labeling. *Stroke* 31: 680–687, 2000.
13. **Clark JM, Sinclair RD, and Lenox JB.** Chemical and nonchemical components of ventilation during hypercapnic exercise in man. *J Appl Physiol* 48: 1065–1076, 1980.
14. **Clark JM, Skolnick BE, Gelfand R, Farber RE, Stierheim M, Stevens WC, Beck G Jr, and Lambertsen CJ.** Relationship of ^{133}Xe cerebral blood flow to middle cerebral arterial flow velocity in men at rest. *J Cereb Blood Flow Metab* 16: 1255–1262, 1996.
15. **Demchenko IT, Oury TD, Crapo JD, and Piantadosi CA.** Regulation of the brain's vascular responses to oxygen. *Circ Res* 91: 1031–1037, 2002.
16. **Detre JA, Leigh JS, Williams DS, and Koretsky AP.** Perfusion imaging. *Magn Reson Med* 23: 37–45, 1992.
17. **Dietrich HH, Ellsworth ML, Sprague RS, and Dacey RG Jr.** Red blood cell regulation of microvascular tone through adenosine triphosphate. *Am J Physiol Heart Circ Physiol* 278: H1294–H1298, 2000.
18. **Faraci FM and Sobey CG.** Role of potassium channels in regulation of cerebral vascular tone. *J Cereb Blood Flow Metab* 18: 1047–1063, 1998.

19. **Floyd T, Maldjian J, Gonzales-Atavales J, Alsop D, and Detre J.** Test-retest stability with continuous arterial spin labeled (CASL) perfusion MRI in regional measurement of cerebral blood flow. *Ninth Annual Meeting of the ISMRM*, Glasgow, UK: ISMRM, 2001, p. 1569.
20. **Floyd TF, McGarvey M, Ochroch EA, Cheung AT, Augoustides JA, Bavaria JE, Acker MA, Pochettino A, and Detre JA.** Perioperative changes in cerebral blood flow after cardiac surgery: influence of anemia and aging. *Annals Thorac Surg*. In press.
21. **Frank LR, Wong EC, Haseler LJ, and Buxton RB.** Dynamic imaging of perfusion in human skeletal muscle during exercise with arterial spin labeling. *Magn Reson Med* 42: 258–267, 1999.
22. **Gessel R.** The regulation of respiration with special reference to the metabolism of the respiratory center and the coordination of the dual function of hemoglobin. *Am J Physiol* 66: 5–49, 1923.
23. **Golanov EV and Reis DJ.** Contribution of oxygen-sensitive neurons of the rostral ventrolateral medulla to hypoxic cerebral vasodilatation in the rat. *J Physiol* 495: 201–216, 1996.
24. **Iida H, Akutsu T, Endo K, Fukuda H, Inoue T, Ito H, Koga S, Komatani A, Kuwabara Y, Momose T, Nishizawa S, Odano I, Ohkubo M, Sasaki Y, Suzuki H, Tanada S, Toyama H, Yonekura Y, Yoshida T, and Uemura K.** A multicenter validation of regional cerebral blood flow quantitation using [^{123}I]iodoamphetamine and single photon emission computed tomography. *J Cereb Blood Flow Metab* 16: 781–793, 1996.
25. **Ishikawa T, Kawamura S, Hadeishi H, Suzuki A, Yasui N, and Uemura K.** Cerebral blood flow and oxygen metabolism in hemiparetic patients with chronic subdural hematoma. Quantitative evaluation using positron emission tomography. *Surg Neurol* 43: 130–137, 1995.
26. **Kety SS and Schmidt CF.** The determination of cerebral blood flow in man by the use of nitrous oxide in low concentrations. *Am J Physiol* 143: 53–66, 1945.
27. **Kety SS and Schmidt CF.** The effects of altered arterial tensions of carbon dioxide and oxygen on cerebral blood flow and oxygen consumption of normal young men. *J Clin Invest* 27: 484–486, 1948.
28. **Kolbitsch C, Lorenz IH, Hormann C, Hinteregger M, Lockinger A, Moser PL, Kremser C, Schocke M, Felber S, Pfeiffer KP, and Benzer A.** The influence of hyperoxia on regional cerebral blood flow (rCBF), regional cerebral blood volume (rCBV) and cerebral blood flow velocity in the middle cerebral artery (CBFVMCA) in human volunteers. *Magn Reson Imaging* 20: 535–541, 2002.
29. **Lambertsen CJ.** Effects of oxygen at high partial pressure. In: *Handbook of Physiology. Respiration*. Bethesda, MD: Am. Physiol. Soc., 1965, sect. 3, vol. II, chapt. 39, p. 1027–1046.
30. **Lambertsen CJ.** Effects of hyperoxia on organs and their tissues. In: *Extrapulmonary Manifestations of Respiratory Disease*, edited by Robin E. New York: Dekker, 1978, p. 239–303.
31. **Lambertsen CJ.** Invited editorial on "Fast and slow components of cerebral blood flow response to step decreases in end-tidal P_{CO_2} in humans." *J Appl Physiol* 85: 386–387, 1998.
32. **Lambertsen CJ, Ewing JH, Kough RH, Gould R, and Stroud MW.** Oxygen toxicity. Arterial and internal jugular blood gas composition in man during inhalation of air, 100% O_2 and 2% CO_2 in O_2 at 3.5 atmospheres ambient pressure. *J Appl Physiol* 8: 255–263, 1955.
33. **Lambertsen CJ, Kough RH, Cooper DY, Emmel GL, Loeschcke HH, and Schmidt CF.** Comparison of relationship of respiratory minute volume to P_{CO_2} and pH of arterial and internal jugular blood in normal man during hyperventilation produced by low concentrations of CO_2 at 1 atmosphere and by O_2 at 3.0 atmospheres. *J Appl Physiol* 5: 803–813, 1953.
34. **Lambertsen CJ, Kough RH, Cooper DY, Emmel GL, Loeschcke HH, and Schmidt CF.** Oxygen toxicity: effects in man of oxygen inhalation at 1 and 3.5 atmospheres upon blood gas transport, cerebral circulation, and cerebral metabolism. *J Appl Physiol* 5: 471–485, 1953.
35. **Lassen N and Lane MH.** Validity of internal jugular blood for study of cerebral blood flow and metabolism. *J Appl Physiol* 16: 313–320, 1960.
36. **Lia TQ, Guang Chen Z, Ostergaard L, Hindmarsh T, and Moseley ME.** Quantification of cerebral blood flow by bolus tracking and artery spin tagging methods. *Magn Reson Imaging* 18: 503–512, 2000.
37. **Liu HL, Kochunov P, Hou J, Pu Y, Mahankali S, Feng CM, Yee SH, Wan YL, Fox PT, and Gao JH.** Perfusion-weighted imaging of interictal hypoperfusion in temporal lobe epilepsy using FAIR-HASTE: comparison with $H_2{}^{15}O$ PET measurements. *Magn Reson Med* 45: 431–435, 2001.
38. **Loeppky JA, Luft UC, and Fletcher ER.** Quantitative description of whole blood CO_2 dissociation curve and Haldane effect. *Respir Physiol* 51: 167–181, 1983.
39. **Mai VM, Bankier AA, Prasad PV, Li W, Storey P, Edelman RR, and Chen Q.** MR ventilation-perfusion imaging of human lung using oxygen-enhanced and arterial spin labeling techniques. *J Magn Reson Imaging* 14: 574–579, 2001.
40. **Ohta H.** [The effect of hyperoxemia on cerebral blood flow in normal humans]. *No To Shinkei* 38: 949–959, 1986.
41. **Pantano P, Baron JC, Lebrun-Grandie P, Duquesnoy N, Bousser MG, and Comar D.** Regional cerebral blood flow and oxygen consumption in human aging. *Stroke* 15: 635–641, 1984.
42. **Pearce WJ.** Mechanisms of hypoxic cerebral vasodilatation. *Pharmacol Ther* 65: 75–91, 1995.
43. **Phillis JW.** Adenosine in the control of the cerebral circulation. *Cerebrovasc Brain Metab Rev* 1: 26–54, 1989.
44. **Pohl U.** Endothelial cells as part of a vascular oxygen-sensing system: hypoxia-induced release of autacoids. *Experientia* 46: 1175–1179, 1990.
45. **Reivich M.** Cerebral circulatory responses to respiratory influences. In: *Cerebral Vascular Diseases*, edited by Toole JF SR, and Whisnant JP. New York: Grune and Stratton, 1968, p. 91–100.
46. **Reivich M.** Regulation of the cerebral circulation. In: *Proceedings of the Congress of Neurological Surgeons*. Baltimore, MD: Williams and Wilkins, 1969, p. 378–418.
47. **Roberts DA, Detre JA, Bolinger L, Insko EK, Lenkinski RE, Pentecost MJ, and Leigh JS Jr.** Renal perfusion in humans: MR imaging with spin tagging of arterial water. *Radiology* 196: 281–286, 1995.
48. **Roberts DA, Rizi RR, Lipson DA, Ferrante MA, Bearn L, Rolf L, Baumgardner J, Yamomoto A, Hatabu H, Hansen-Flaschen J, Gefter WB, and Schnall MD.** Dynamic observation of pulmonary perfusion using continuous arterial spin-labeling in a pig model. *J Magn Reson Imaging* 14: 175–180, 2001.
49. **Rostrup E, Larsson HB, Toft PB, Garde K, and Henriksen O.** Signal changes in gradient echo images of human brain induced by hypo- and hyperoxia. *NMR Biomed* 8: 41–47, 1995.
50. **Scheinberg P.** The effect of nicotinic acid on the cerebral circulation with observations on extracranial contamination of cerebral venous blood in the nitrous oxide procedure for cerebral blood flow. *Circulation* 1: 1148–1154, 1950.
51. **Sharan M, Gupta S, and Popel AS.** Parametric analysis of the relationship between end-capillary and mean tissue P_{O_2} as predicted by a mathematical model. *J Theor Biol* 195: 439–449, 1998.
52. **Shenkin HA, Harmel MH, and Kety SS.** Dynamic anatomy of the cerebral circulation. *Arch Neurol Psychiatry* 60: 240–252, 1948.
53. **Siesjo BK.** Measurements of cerebral oxygen consumption: advantages and limitations. *Eur Neurol* 20: 194–199, 1981.
54. **Silva AC, Kim SG, and Garwood M.** Imaging blood flow in brain tumors using arterial spin labeling. *Magn Reson Med* 44: 169–173, 2000.

54a. *Statistical Parametric Mapping 99: Wellcome Department of Cognitive Neurology*, 2000.

55. **Swenson ER, Robertson HT, and Hlastala MP.** Effects of inspired carbon dioxide on ventilation-perfusion matching in normoxia, hypoxia, and hyperoxia. *Am J Respir Crit Care Med* 149: 1563–1569, 1994.
56. **Walsh EG, Minematsu K, Leppo J, and Moore SC.** Radioactive microsphere validation of a volume localized continuous saturation perfusion measurement. *Magn Reson Med* 31: 147–153, 1994.

57. **Wang J, Alsop DC, Song HK, Maldjian JA, Tang K, Rabin M, Schnall MD, and Detre JA.** Arterial transit-time imaging with flow encoding arterial spin tagging (FEAST). *Magn Reson Med* 50: 599–607, 2003.
58. **Waschke KF, Krieter H, Hagen G, Albrecht DM, Van Ackern K, and Kuschinsky W.** Lack of dependence of cerebral blood flow on blood viscosity after blood exchange with a Newtonian O_2 carrier. *J Cereb Blood Flow Metab* 14: 871–876, 1994.
59. **Watson NA, Beards SC, Altaf N, Kassner A, and Jackson A.** The effect of hyperoxia on cerebral blood flow: a study in healthy volunteers using magnetic resonance phase-contrast angiography. *Eur J Anaesthesiol* 17: 152–159, 2000.
60. **Wolf RL, Alsop DC, Levy-Reis I, Meyer PT, Maldjian JA, Gonzalez-Atavales J, French JA, Alavi A, and Detre JA.** Detection of mesial temporal lobe hypoperfusion in patients with temporal lobe epilepsy by use of arterial spin labeled perfusion MR imaging. *AJNR Am J Neuroradiol* 22: 1334–1341, 2001.
61. **Wong EC.** Potential and pitfalls of arterial spin labeling based perfusion imaging techniques for MRI. In: *Functional MRI*, edited by Moonen CTW and Bandettini PA. Heidelberg, Germany: Springer-Verlag, 1999, p. 63–69.
62. **Wong EC, Buxton RB, and Frank LR.** Implementation of quantitative perfusion imaging techniques for functional brain mapping using pulsed arterial spin labeling. *NMR Biomed* 10: 237–249, 1997.
63. **Wong EC, Buxton RB, and Frank LR.** Quantitative perfusion imaging using arterial spin labeling. *Neuroimaging Clin N Am* 9: 333–342, 1999.
64. **Xu Y, Liachenko S, and Tang P.** Dependence of early cerebral reperfusion and long-term outcome on resuscitation efficiency after cardiac arrest in rats. *Stroke* 33: 837–843, 2002.
65. **Ye FQ, Berman KF, Ellmore T, Esposito G, van Horn JD, Yang Y, Duyn J, Smith AM, Frank JA, Weinberger DR, and McLaughlin AC.** $H_2{}^{15}O$ PET validation of steady-state arterial spin tagging cerebral blood flow measurements in humans. *Magn Reson Med* 44: 450–456, 2000.